Appl Nanosci (2015) 5:673–680
DOI 10.1007/s13204-014-0363-9

ORIGINAL ARTICLE

Synthesis and characterization of $CdS/CuAl_2O_4$ core–shell: application to photocatalytic eosin degradation

B. Bellal · M. Trari · A. Afalfiz

Received: 7 May 2014 / Accepted: 22 September 2014 / Published online: 25 October 2014

Abstract The advantages of the hetero-junction $CdS/CuAl_2O_4$ for the photocatalytic eosin degradation are reported. Composite semiconductors are elaborated by co-precipitation of CdS on the spinel $CuAl_2O_4$ giving a core–shell structure with a uniform dispersion and intimate contact of the spinel nanoparticles inside the hexagonal CdS. The Mott–Schottky plots (C^{-2}–V) of both materials show linear behaviors from which flat band potentials are determined. The photoactivity increases with increasing the mass of the sensitizer CdS and the best performance is achieved on $CdS/CuAl_2O_4$ (85 %/15 %). The pH has a strong influence on the degradation and the photoactivity peaks at pH 7.78. The dark adsorption eosin is weak ($\sim$4 %), hence the change in the eosin concentration is attributed to the photocatalytic process. The degradation follows a zero-order kinetic with a rate constant of 5.2×10^{-8} mol L^{-1} mn^{-1} while that of the photolysis is seven times lower (0.75×10^{-8} mol L^{-1} mn^{-1}).

Keywords Hetero-junction $CdS/CuAl_2O_4$ · Core–shell · Eosin · Photocatalytic degradation

Introduction

In view of growing demand of the energy and increasing cost for the water treatment, the exploitation of the solar energy is highly recommended (Bassaid et al. 2009; Zou and Zhu 2008) because of its cleanliness, abundance (1,250 W m^{-2}, Sahara), consistency and renewability. The applications of the photocatalysis are varied and it is the environmental aspect that we develop through the eosin degradation. The presence of dyes, even at low concentrations, disturbs the ecosystem and decreases the transparency of water, thus affecting dramatically the photosynthesis and in this way the aquatic life (Petrov and Stoichev 2002; Hongwen 2010). So, the effluents must be treated before discharge and an ideal treatment should mineralize the organic matter without leaving any hazardous molecules. In this respect, the advanced oxidation process (AOP) has emerged as a promising technique for the environmental protection (Qamar et al. 2009) and is actively used to degrade a variety of dyes and pesticides (Yahiat et al. 2011). The oxygen plays undoubtedly a crucial role in the dyes oxidation (Arsac et al. 2008) and the reactive radicals are responsible of the photodegradation through AOP (Arslan-Alaton 2007).

The semiconductor (SC) oxides are currently used in photocatalysis (Sahoo et al. 2014). Unfortunately, many of them are inappropriate as a result of large gap and improper position of the band edges which do not span the redox levels in solution and only fewer compounds fulfilling all photo-electrochemical (PEC) characteristics have been found nowadays. Accordingly, there has been many works in the development of new optically active materials, and the spinels CuM_2O_4 are reported to be efficient photocatalysts, responsive to visible light (Takimoto et al. 2012). However, the major drawback comes from the short lifetime of the charge carriers. Indeed, the rate determining step in heterogeneous charge transfer involves the carriers flow in narrow $3d$ bands ($\sim$2 eV) and the spinels suffer from a lost of electron/hole (e^-/h^+) pairs originating from

B. Bellal · M. Trari (✉) · A. Afalfiz
Laboratory of Storage and Valorization of Renewable Energies
Faculty of Chemistry, University of Sciences and Technology (USTHB), BP 32, 16111 Algiers, Algeria
e-mail: solarchemistry@gmail.com

B. Bellal
e-mail: bachirbellal60@gmail.com

the low carriers mobility (Bellal et al. 2009). Then, the question arises about the effect of decreasing the dimension of the crystallite on the catalytic activity. The crystallite size must be comparable with the diffusion length of the minority carriers and the chemical route is appropriate for the synthesis of nanocrystallites (Yang et al. 2009; Benreguia et al. 2011). $CuAl_2O_4$ has environmentally friendly characteristics, in addition to be chemically stable, low cost and absorbs over the whole solar spectrum.

On the other hand, the photocatalysis remains limited to simple materials and there have been some strategies aimed to improve the PEC performance (Mekatel et al. 2012). A straightforward solution would be the utilization of hetero-junctions (Belhadi et al. 2011) where little systematic work with the spinels has been done because of the difficulty of adjusting the electronic bands of SCs. The hetero-junction could not only extend the spectral response of wide band gap SCs toward lower energies but also favors the charge separation by increasing the lifetime of the charge carriers. CdS has been tested successfully as photocatalyst (Ge and Liu 2011) and its activity is significantly improved when it supports narrow band gap SCs. Our group has been working on the dyes photodegradation (Bessekhouad et al. 2012) and in continuation we report the photooxidation of eosin over the novel hetero-system $CdS/CuAl_2O_4$. Eosin is a model molecule and the aim consists at studying the influence of the mass and pH to find the optimal conditions for the best photoactivity. The major challenge is to deposit the spinel nanocrystallites inside CdS by co-precipitation.

Experimental

$CuAl_2O_4$ is synthesized by nitrate route which has succeeded in the preparation of spinels (Zhu et al. 2012). $Al(NO_3)_3{,}9H_2O$ (Merck) and CuO (Merck, pre-fired at 400 °C), both of purity greater than 99.5 %, are used as starting reagents. The stochiometric mixture is dissolved in HNO_3 (Sigma Aldrich 69 %); the solution is evaporated and heated on a hot plate until there are no NO_x fumes. The amorphous powder is fired at 950 °C in air and furnace cooled; the end product exhibits a brown color. CdS is prepared by precipitation using thiourea as sulphide source; $CdSO_4$, $8/3H_2O$ (PRS Panreac) is dissolved in bi-distilled water and complexed with ammonia (Panreac 30 %) in a three-neck round-bottom flask (500 mL capacity). Thiourea solution contained in a pressure-equalizing dropping funnel is added drop wise to the $Cd(NH_3)_4^{2+}$ solution and the mixture is maintained under reflux at 85 °C. CdS is recovered by filtration on a Millipore filter (0.45 μm), thoroughly rinsed with water, then with ethanol and dried overnight at 110 °C. The hetero-junction is prepared by core–shell (Ghows and Entezari 2012): $CuAl_2O_4$ powder is added under agitation to the $Cd(NH_3)_4^{2+}$ solution before thiourea. All compositions (0–50 wt.%) are further degassed under vacuum at 100 °C to evacuate the physisorbed water. The CdS powder (~300 mg) is cold pressed into pellets under 2 kbar, sealed in evacuated Pyrex tube (<1 mbar), heated at 650 °C (3 h) and water quenched to have the hexagonal polymorph; the compactness of the pellets is ~70 %.

X-ray diffraction (XRD) is carried out with a Phillips diffractometer using Cu Kα radiation; the 2θ range is (15–90°) with a step 0.02° and scanning time of 1 s. The size of the crystallites is evaluated from the full width at half maximum using Xpowder software and the Williamson–Hall plot. The morphology of the hetero-junction is examined by scanning electron microscopy (SEM, Nicoplet 235) working at 20 kV. The diffuse reflectance spectra are recorded with a UV–Vis spectrophotometer (Specord 200 Plus). The collected data ($R_\infty = R_{sample}/R_{reference}$) are converted using the Kubelka–Munk relation:

$$F(R_\infty) = (1 - R_\infty)^2/2R_\infty) \quad (1)$$

The point of zero charge (pzc) is determined by measuring the equilibrium pH of an aqueous solution containing a suspension of finely powdered sample. To minimize the contact resistance, silver cement is deposited on the back pellets by spot welding copper wires. The pellets are encapsulated in glass holders with epoxy resin leaving a projected surface area of 1.32 cm^2. PEC measurements are done under potentiostatic mode using a standard cell in Na_2SO_4 (0.5 M, pH ~ 7) solution as indifferent salt and eosin at various concentrations; the solution is not purged prior the measurement. Pt electrode is used as auxiliary electrode and the potential is monitored by a PGZ 301 potentiostat (Radiometer analytical) and given with respect to a saturated calomel electrode (SCE). The electrode is illuminated through an optical window with a 150 W halogen lamp, positioned at 0.5 cm to minimize the light absorption by the solution. The variation of the interfacial capacitance with the applied potential is measured at a frequency of 10 kHz.

Typically, 0.5 g L^{-1} of the catalyst is suspended in 200 mL of eosin solution (10 ppm) in a Pyrex reactor open at atmospheric pressure and equipped with a cooling system. The percentage of $CuAl_2O_4$ in the hetero-junction is given with respect to CdS. The initial pH is adjusted to the desired value by addition of NaOH or H_2SO_4 solutions. The temperature is regulated at 25 °C and the suspension is maintained overnight in the dark to ensure complete adsorption. The visible light is provided by 150 W halogen lamp, positioned above the reactor (12 mW cm^{-2}). During

the course of the reaction, 5 mL of the powder suspension is withdrawn at regular time intervals to maintain the solid/liquid ratio constant. The suspension is subjected to a strong centrifugation (3,000 rpm, 10 mn) to remove the solid particles. The residual concentration of eosin is measured with a double beam spectrophotometer (Shimadzu 1800, $\lambda_{max} = 516$ nm) using 1 cm quartz cell. The electrons injection from eosin to CdS is studied by plotting the intensity-potential J(V) curves at various eosin concentrations (Asha Jhonsi et al. 2009). Filtered light through a band-pass filter (600 nm) is used to check the absence of electrons transfer from the spinel to CdS. The catalyst shows no evidence of cadmium dissolution after 5 h illumination. All solutions are made up with CO_2 free bi-distilled water (~ 1 MΩ cm).

Results and discussion

To prevent CdS oxidation, the heat treatment is performed in evacuated silica ampoule at 650 °C. A polymorphic transition from the cubic phase (greenockite, SG: $P6_3mc$) to the hexagonal phase (Hawletite, SG: F43m) occurs at ~450 °C under inert atmosphere. Nevertheless, the reverse transition is so sluggish that the hexagonal form is easily obtained by water quenching. The XRD pattern of the hetero-junction shows a mixture of the normal spinel $Cu[Al]_2O_4$ and hexagonal CdS (Fig. 1) in agreement with the JCPDS cards No 33-0448 and 41-1049 respectively. The crystallite size (D) is a crucial parameter which significantly affects the photoactivity of small polaron SCs. Therefore, we have used the chemical route for preparing the bi-functional catalyst. The crystallite size of CdS (35.81 ± 9.96 nm) is evaluated by extrapolation to $\theta = 0$ using the Williamson–Hall plot (Xpowder software) (Table 1).

The SEM picture of the core–shell structure CdS/$CuAl_2O_4$ (Fig. 2) shows that all grains have sub-spherical form where the white CdS crowns are surrounded by the gray spinel. The diffuse reflectance spectra of the catalysts are shown in Fig. 3. The absorption edge of the hetero-system does not shift with respect to CdS indicating the absence of quantum size effect. Similar results have already been obtained on the preparation of CdS/Al-HMS nanocomposites (Zhang and Zhang 2009). Unlike XRD results, the absorption of the spinel is masked in the core–shell structure because of the low penetration length of the UV–Visible light in CdS attributed to the high absorption coefficient. The spectra of CdS and CdS/$CuAl_2O_4$ core shell are very similar and this clearly indicates that the spinel is coated by CdS. By contrast, the spectrum of the mixture (CdS + $CuAl_2O_4$) presents a hump at longer wavelengths (Fig. not shown).

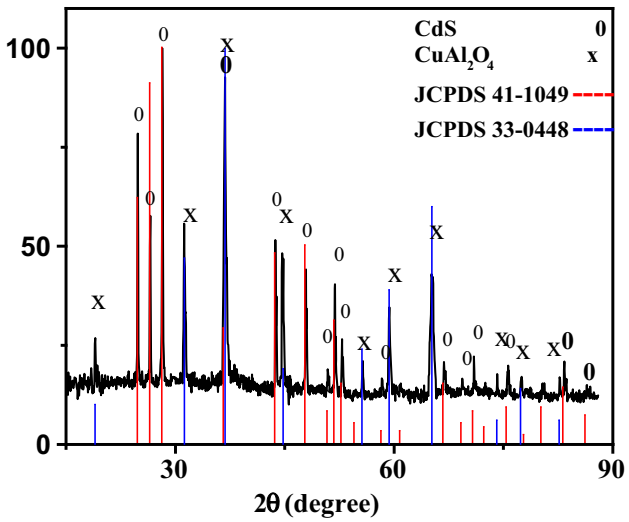

Fig. 1 X-ray diffraction of the hetero-junction CdS/$CuAl_2O_4$ (85/15) in a core–shell structure

The photodegradation of dyes is critically dependent on the position of the electronic bands of SCs. Therefore, it would be logical to start the study by PEC characterization; this was done to establish the energy band diagram for the thermodynamic prevision of interfacial reactions. The photocurrent (J_{ph}) of CdS starts to flow at −1.09 V (photocurrent onset potential V_{on}) and increases toward anodic potentials (Fig. 4, Inset), indicating n-type conductivity. The flat band potential (V_{fb}) is accurately obtained from the capacitance:

$$C^{-2} = \pm\left(\frac{2}{Ae\varepsilon\varepsilon_o N_{D/A}}\right)\left(V - V_{fb} - \frac{kT}{e}\right) \quad (2)$$

where the positive sign is for n-type and the negative sign for p-type specimen. A is the exposed surface area, $N_{D/A}$ the concentrations of donor/acceptor respectively, e the electron charge and kT the thermal energy (~26 meV at 300 K). The permittivity of CdS (ε ~ 6) is taken from the literature (Seoudi et al. 2012). The characteristics (C^{-2}–V) fit linearly with the experimental data; the potentials V_{fb} and the carriers densities are provided from the intercept of the V-axis and the slope respectively (Fig. 4); they are gathered in Table 1 along with the main physical properties.

Photocatalysis

The photocatalysis is efficient for the dyes removal (Mozia 2010) and has attracted a great attention as an environmentally friendly technique for the water treatment (Khataee and Zarei 2011). Some strategies have been reported to increase the quantum yield; the hetero-junctions are actively used for the water remediation and AOP occurs through radicals $O_2^{\bullet}$ and/or $OH^{\bullet}$, able to attack the organic

Table 1 The main physical properties of $CuAl_2O_4$ and CdS

	Structure	Crystallite size (nm)	Color	E_g (eV)	Type	V_{fb} (V_{SCE})	E_{CB} (V_{SCE})	pzc
$CuAl_2O_4$	Cubic: Fd3 m	35.81 ± 9.96	Brown	1.70	*p*	−1.05	−1.21	7.6
CdS	Hexagonal: $P6_3mc$	38.71 ± 2.81	Yellow	2.41	*n*	−1.02	−1.03	–

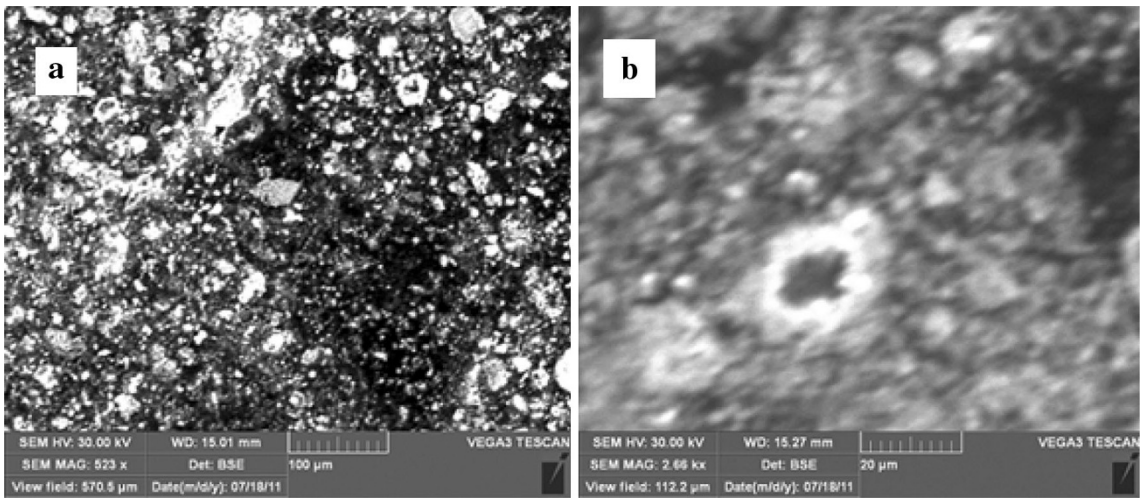

Fig. 2 SEM micrograph of core–shell hetero-junction $CdS/CuAl_2O_4$ (85/15)

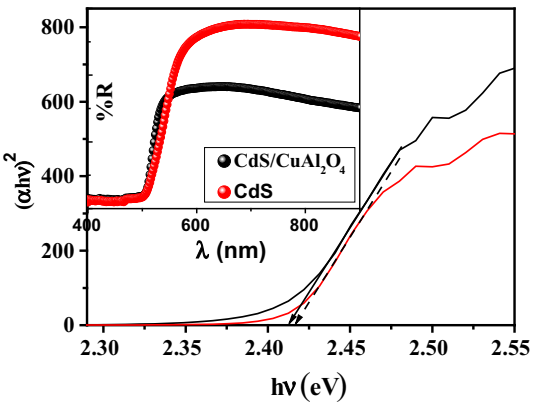

Fig. 3 The direct optical transition of CdS and the hetero-junction $CdS/CuAl_2O_4$ (85/15) in the core–shell structure. *Inset* the diffuse reflectance spectra

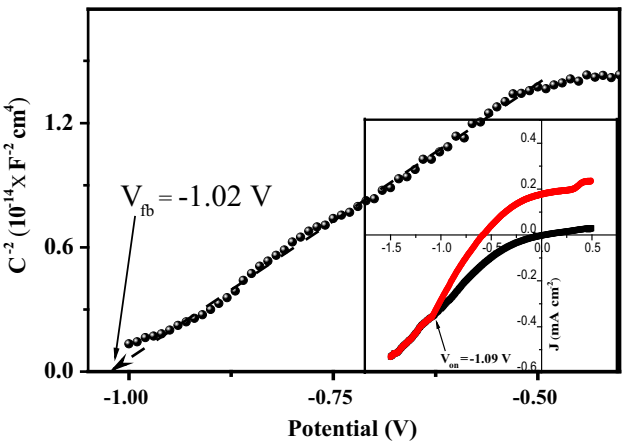

Fig. 4 The Mott–Schottky plot of CdS in neutral solution (Na_2SO_4, 10^{-3} M). *Inset* the J(V) curves in the *dark* and under illumination

matter until total mineralization. The energy diagram of the hetero-junction $CdS/CuAl_2O_4$/eosin solution (Fig. 5a), established from the PEC characterization is a main pre-requisite for PEC applications. Both CdS-CB and $CuAl_2O_4$-CB are pH-insensitive. Therefore, their difference in the hetero-junction measures the band bending and the pH effect comes rather from the interface CdS/solution. Eosin is preferentially adsorbed on dS surface where the photooxidation occurs and the pH plays a crucial role through pzc. Indeed, a strong adsorption should favor the oxidation and the solution is equilibrated with the powder in the dark. Hence, the amount of adsorbed eosin is proportional to the active surface and its attachment allows the electron transfer under illumination. At high pHs (>pzc), the CdS surface has a negative charge attributed to a large fraction of active sites and the interaction between eosin and CdS is achieved by electrostatic attraction through anchoring carboxylic function. Due to the nanomorphology of CdS, the distance travelled by the photoelectrons is reduced to less than 40 nm. Accordingly, the depletion width becomes so small that the electrons move to the interface by diffusion. Alone, $CuAl_2O_4$ exhibits no activity

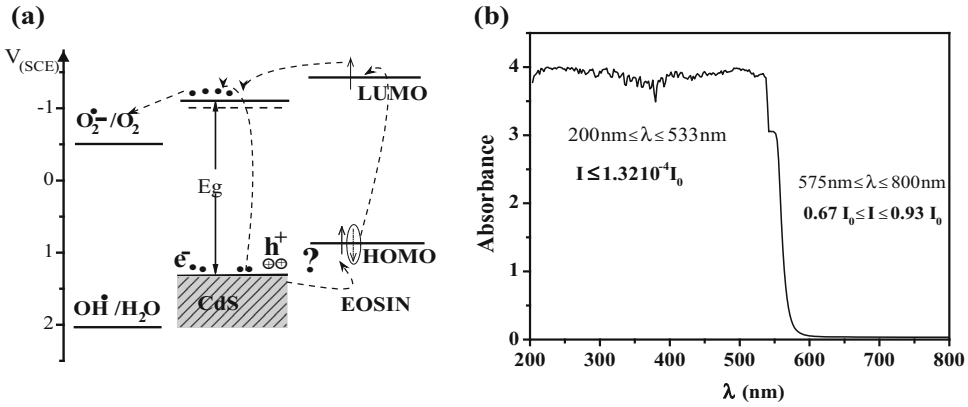

Fig. 5 **a** The energy band diagram of CdS and the energy levels of eosin. **b** The absorption spectrum of the filter showing the injection phenomenon

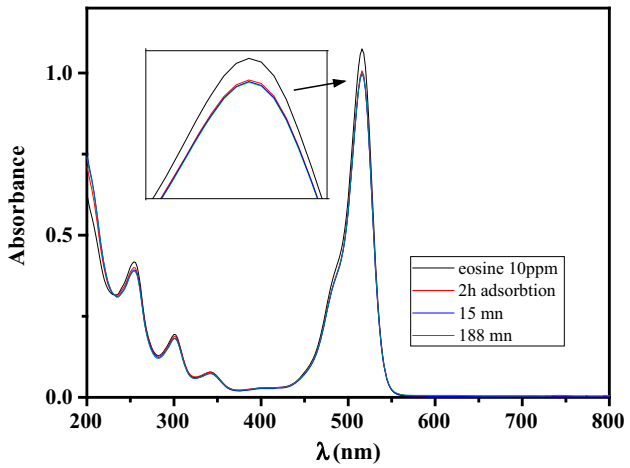

Fig. 6 The spectra of eosin under filtered light in presence of the hetero-junction (see text)

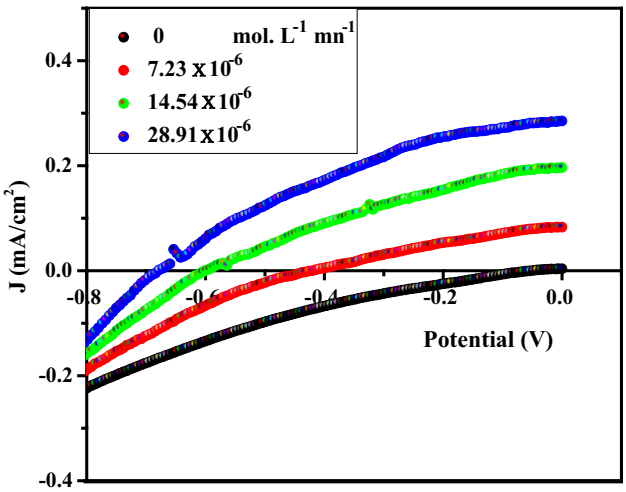

Fig. 7 The J(V) curves of CdS in eosin solutions at different concentrations, indicating the injection process

but when coupled to CdS, the performance increases significantly. As noticed above, the hetero-junction shifts the spectral photo response of CdS toward longer wavelengths and hinders the recombination of (e^-/h^+) pairs. The electrons in CdS-CB (−1.10 V) have enough cathodic potential to generate radicals $O_2^\bullet$ from dissolved oxygen because of the less cathodic potential of the couple $O_2/O_2^\bullet$ (−0.52 V). By contrast, the diagram clearly shows that the photoholes do not participate in the photoactivity because the potential of the couple $OH^\bullet/H_2O$ (2.03 V) is more anodic than CdS-VB.

The question to be settled is whether or not $CuAl_2O_4$ injects electrons into CdS-CB. To answer this question, we have used filtered light (650 nm) whose spectrum is given in Fig. 5b. Contrary to what is commonly believed and although the good position of the conduction bands of both SCs, no injection is observed as evidenced from the absence of photoactivity and this remains a puzzle to solve, the results are well illustrated in Fig. 6 where there is no difference between the spectra of the initial concentration (10 ppm), the solutions after 2 h of adsorption and 3 h of illumination. Based on our findings and considering the results of the literature (Chhor et al. 2004), the eosin oxidation occurs by radicals:

$$O_{2ads} + e^- \rightarrow O_2^\bullet + (H^+) \rightarrow HO_2^\bullet \rightarrow H_2O_2 (+ e^-) \rightarrow O_2 + OH^\bullet + OH^- \quad (3)$$

It has been reported that hydrogen peroxide works as electron acceptor, thus promoting the production of reactive $OH^\bullet$ (Lahmar et al. 2012). As mentioned above, it is unlikely for water to be oxidized due to its extremely high overvoltage on CdS. The enhanced activity is explained by the energy levels of CdS, the electrons and holes form respectively $O_2^\bullet$ and/or $OH^\bullet$ radicals under illumination Chhor et al. (2004):

$$CdS + h\nu \rightarrow CdS - CB\ (e^-) + CdS - VB\ (h^+) \quad (4)$$

$$CdS - CB\ (e^-) + O_2 \rightarrow O_2^{\bullet -} \quad (5)$$

thus allowing an increase of the lifetime of (e^-/h^+) pairs and in this way an enhancement of the photoactivity. Oxygen is reduced preferentially to form radicals $O_2^\bullet$.

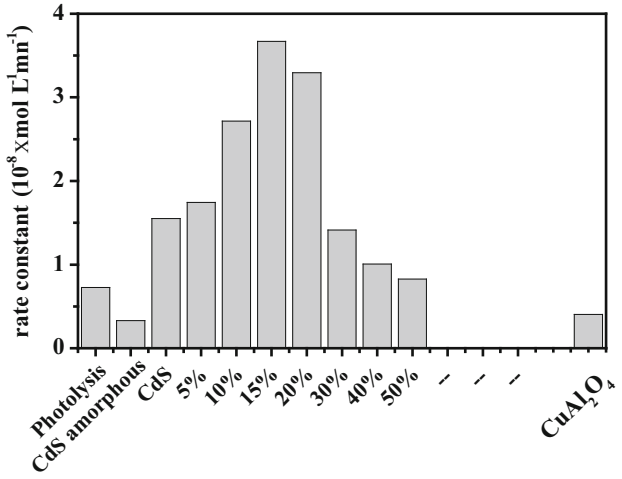

Fig. 8 Histogram of the rate constants of eosin degradation on different catalysts along with the photolysis

Therefore, if the solution is purged with nitrogen, the eosin degradation is strongly inhibited.

On the other hand, CdS is made responsive to longer wavelengths by adhering the dye molecules on its surface, making the electron transfer from excited eosin to CdS-CB possible. An injection from eosin to CdS has been experimentally observed through the intensity-potential J(V) plots (Fig. 7). The increase of the current with increasing the eosin concentration clearly indicates that the energy of excited state (LUMO) of eosin is located above CdS-CB. This hypothesis is corroborated by the recent work of Jhonsi et al. where the LUMO and HOMO levels of eosin are found to be −1.45 and +0.86 V respectively (Asha Jhonsi et al. 2009).

The electronic bands of the spinel $CuAl_2O_4$ are pH insensitive, therefore it is thermodynamically possible for holes to be injected in $CuAl_2O_4$-VB but this hypothesis has not been checked in our case. Another possibility is the holes injection from CdS-VB to the less anodic single state of eosin (HOMO level), owing to the difference {CdS-VB − eosin (HOMO) = 0.45 V}. In addition, the redox potential of the eosin couple S^+/S (+0.86 V) permits the eosin oxidation. Such hypothesis is not easy to check by filtered light because of the closeness of the gap of CdS (2.42 eV) and the quantity {LUMO − HOMO = 2.40 eV). However, such hypothesis could be checked by the corrosion study. In absence of injection, the holes corrode the CdS lattice and liberate Cd^{2+} {$CdS + 2\ h^+ \rightarrow Cd^{2+} + S$}.

The eosin has a large extinction coefficient and the light absorption is restricted to only few layers. So, there is an optimal concentration above which eosin acts as optical filter and inhibits the photocatalysis; the light is absorbed before reaching the catalyst and competes with SCs absorption, thus lowering considerably the photoactivity.

The photoactivity depends on the mass of $CuAl_2O_4$ and $CdS/CuAl_2O_4$ (85 %/15 %), gives the higher performance (Fig. 8). The ability of CdS to inject electrons to dissolved oxygen is function of pH. Several pHs have been tested and the curve is fitted according to a Gaussian regression over the pH range (4–12) with a maximal pH of 7.78 (Fig. 9a) and a rate constant ($k_{\text{theo.}} = 5.29 \times 10^{-7}$ mol L^{-1} mn^{-1}), this pH has been checked experimentally in our case and the photoactivity gave a very close value of 7.78 (9b) with an experimental constant ($k_{\text{exp.}}$) of 5.20×10^{-7} mol L^{-1} mn^{-1}. The photo catalytic yield is calculated from the relation:

$$\eta = (C_o - C_t/C_o) \times 100 \quad (6)$$

where C_o is the initial concentration and C_t the concentration at the time (t). The linear relation between C_t and illumination time (t) indicates that the degradation follows a zero-order kinetic with a rate constant of 5.2×10^{-7} mol L^{-1} mn^{-1}. It is worthwhile to outline that the rate constant of the photolysis (in absence of the catalyst) is seven times smaller (0.75×10^{-7} mol L^{-1} mn^{-1}).

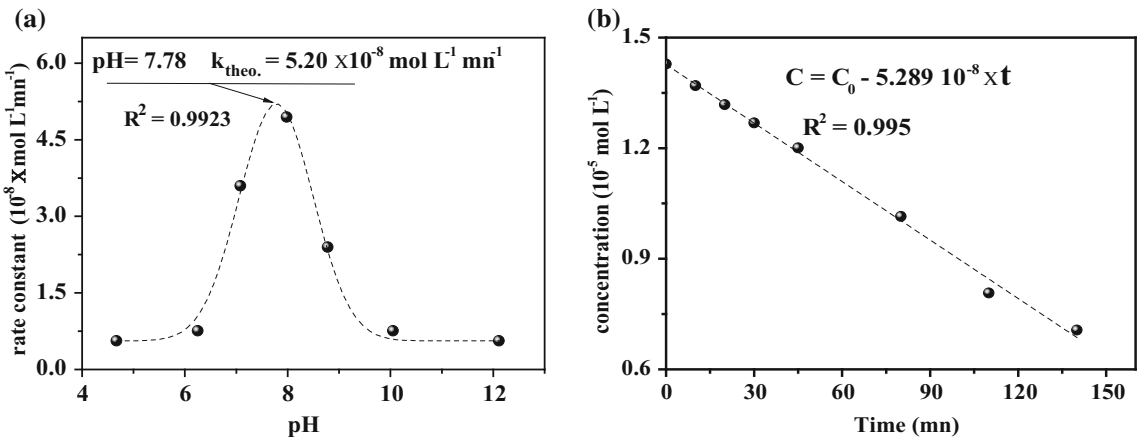

Fig. 9 **a** The pH optimization of the eosin degradation. **b** The experimental rate constants at the optimal pH (7.78)

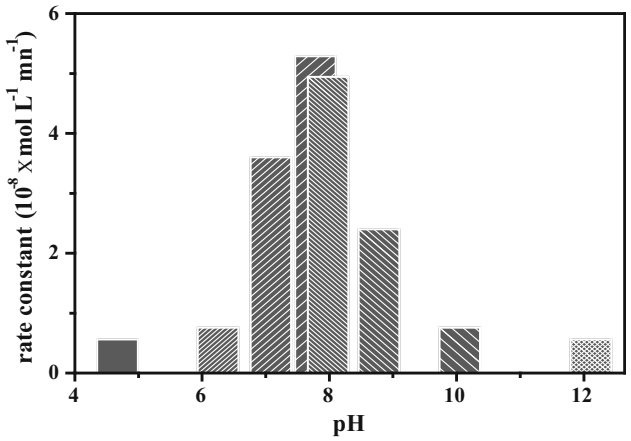

Fig. 10 Histogram of the rate constants of eosin degradation on the hetero-junction $CdS/CuAl_2O_4$ (85/15) at different pHs

The best activity is obtained on $CdS/CuAl_2O_4$ (85 %/15 %)/eosin (10 ppm) at pH 7.98 (Fig. 6). The eosin oxidation occurs via several paths and this requires a deep investigation like combined HPLC/GCMS and total organic carbon. The work is presently under way and the results will be reported consecutively (Fig. 10).

Conclusion

Eosin-assisted photooxidation on $CdS/CuAl_2O_4$ is studied under visible light. The low cost, photocatalytic performance and chemical stability at neutral pH make the hetero-junction attractive. The spinel, elaborated by nitrate route, is embedded within the spherical CdS grains giving core–shell structure. The degradation is accelerated by dissolved oxygen. The photoelectrons of CdS react with molecular oxygen to generate $O_2^{\bullet}$ radicals responsible of the eosin oxidation. Although CdS-CB is more cathodic than $CuAl_2O_4$-CB, no electron transfer is observed. By contrast, the current potential curves using optical filter have shown the electron injection from ground state of eosin to conduction band of CdS.

Acknowledgments The authors acknowledge the assistance of Dr Y. Belaroussi in the XRD and SEM experiments. The work was financially supported by the Faculty of Chemistry (Algiers).

References

Arsac F, Bianchi D, Chevelon JM, Conchon P, Ferronato C, Lair A, Sleiman M (2008) Photocatalytic degradation of organic pollutants in water and in air: an analytical approach. Mater Sci Eng C 28:722–725

Arslan-Alaton I (2007) Degradation of a commercial textile biocide with advanced oxidation process and ozone. J Environ Manage 82:145–154

Asha Jhonsi M, Kathiravan A, Renganathan R (2009) Photoinduced interaction between xanthene dyes and colloidal CdS nanoparticles. J Mol Struct 921:279–284

Bassaid S, Chaib M, Omeiri S, Bouguelia A, Trari M (2009) Photocatalytic reduction of cadmium over $CuFeO_2$ synthesized by sol-gel. J Photochem Photobiol A 201:62–68

Belhadi A, Boumaza S, Trari M (2011) Photoassisted hydrogen production under visible light over NiO/ZnO hetero-system. Appl Energy 88:4490–4495

Bellal B, Saadi S, Koriche N, Bouguelia A, Trari M (2009) Physical properties of the delafossite $LaCuO_2$. J Phys Chem Solids 70:1132–1136

Benreguia N, Omeiri S, Bellal B, Trari M (2011) Visible light induced $H_2PO_4^-$ removal over $CuAlO_2$ catalyst. J Hazard Mater 192:1395–1400

Bessekhouad Y, Brahimi R, Hamdini F, Trari M (2012) Cu_2S/TiO_2 heterojunction applied to visible light Orange II degradation. J Photochem Photobiol A 248:15–23

Chhor K, Bocquet JF, Colbeau-Justin C (2004) Comparative studies of phenol and salicylic acid photocatalytic degradation: influence of adsorbed oxygen. Mater Chem Phys 86:123–131

Ge L, Liu J (2011) Efficient visible light-induced photocatalytic degradation of methyl orange by QDs sensitizedCdS-Bi_2WO_6. Appl Catal B 105:289–297

Ghows N, Entezari MH (2012) Sono-synthesis of core–shell nanocrystal (CdS/TiO_2) without surfactant. Ultrason Sonochem 19:1070–1078

Khataee AR, Zarei M (2011) Photocatalysis of a dye solution using immobilized ZnO nanoparticles combined with photoelectrochemical process. Desalination 273:453–460

Lahmar H, Kebir M, Nasrallah N, Trari M (2012) Photocatalytic reduction of Cr(VI) on the new hetero-system $CuCr_2O_4$/ZnO. J Mol Catal A Chem 353–354:74–79

Mekatel H, Amokrane S, Bellal B, Trari M, Nibou D (2012) Photocatalytic reduction of Cr(VI) on nanosized Fe_2O_3 supported on natural Algerian clay: characteristics, kinetic and thermodynamic study. Chem Eng J 200–202:611–618

Mozia S (2010) Application of temperature modified titanate nanotubes for removal of an azo dye from water in a hybrid photocatalysis-MD process. Catal Today 156:198–207

Petrov S, Stoichev PA (2002) Reagent ultrafiltration purification of water contaminated with reactive dyes. Filtr Sep 39:35–38

Qamar M, Gondal MA, Yamani ZH (2009) Synthesis of highly active nanocrystalline WO_3 and its application in laser-induced photocatalytic removal of a dye from water. Catal Commun 10:1980–1984

Sahoo R, Roy A, Ray C, Mondal C, Negishi Y, Yusuf SM, Pal A, Pal T (2014) Decoration of Fe_3O_4 base material with Pd loaded CdS nanoparticle for superior photocatalytic efficiency. J Phys Chem 118(21):11485–11494

Seoudi R, Shabaka AA, Kamal M, Abdelrazek EM, Eisa W (2012) Dependence of spectroscopic and electrical properties on the size of cadmium sulfide nanoparticles. Physica E 45:47–55

Takimoto Y, Kitta T, Irie H (2012) Visible-light sensitive hydrogen evolution photocatalyst $ZnRh_2O_4$. Int J Hydrog Energy 37:134–138

Yahiat S, Fourcade F, Brosillon S, Amrane A (2011) Photocatalysis as a pre-treatment prior to a biological degradation of cyproconazole. Desalination 281:61–67

Yang H, Yan J, Lu Z, Cheng X, Tang Y (2009) Photocatalytic activity evaluation of tetragonal $CuFe_2O_4$ nanoparticles for the H_2 evolution under visible light irradiation. J Alloy Compd 476:715–719

Yu H, Fugetsu B (2010) A novel adsorbent obtained by inserting carbon nanotubes into cavities of diatomite and applications for organic dye elimination from contaminated water. J Hazard Mater 177:138–145

Zhang YJ, Zhang L (2009) Preparation of Ru-loaded CdS/Al-HMS nanocomposites and production of hydrogen by photocatalytic degradation of formic acid. Appl Surf Sci 255:4863–4866

Zhu Z, Zhao Q, Li X, Li Y, Sun C, Zhang G, Cao Y (2012) Photocatalytic performances and activities of $ZnAl_2O_4$ nanorods loaded with Ag towards toluene. Chem Eng J 203:43–51

Zou L, Zhu B (2008) The synergistic effect of ozonation and photocatalysis on color removal from reused water. J Photochem Photobiol A 196:24–32